Transition Metal Chemistry (2021) 46:111–120
https://doi.org/10.1007/s11243-020-00427-3

Coordination of the natural ligand lapachol to iron(II): synthesis, theoretical study and antiproliferative activity

Tamires D. de Oliveira[1,2] · Natália A. Cabeza[1,2] · Gelson T. S. T. da Silva[3] · Ana L. T. G. Ruiz[4] · Anderson R. L. Caires[5] · Rafael G. da Silveira[6] · Daniela C. M. Rodrigues[1] · Antônio R. Fiorucci[2] · Ademir dos Anjos[1,2]

Received: 24 May 2020 / Accepted: 19 September 2020 / Published online: 7 October 2020

Abstract

Lapachol is a natural naphthoquinone known for having a variety of biological properties, and in recent years, it has been used in the synthesis of metal complexes with biological applications. This work reports on the synthesis, properties and antiproliferative activity of one new metal complex obtained by the reaction of the natural naphthoquinone lapachol with Fe(II). Characterizations by CHN elemental analysis, electrochemical and spectroscopic techniques (infrared, UV–Vis and luminescence) allowed to infer the coordination of two lapachol molecules to the metallic Fe(II) ion through the phenolic and carbonyl oxygens, as well as the presence of two water molecules completing the complex coordination sphere. Molecular modeling was in good agreement with the $[Fe(Lap)_2(H_2O)_2]\cdot 2H_2O$ complex structure proposed from the experimental data. Antiproliferative activity assay revealed the efficiency of the $[Fe(Lap)_2(H_2O)_2]\cdot 2H_2O$ complex against some human tumor cell lines, with lowest TGI (Total growth inhibition) value and higher selectivity index for the glioma tumor cell line (U251).

Introduction

In the last decades, research on compounds for cancer treatment been intensified because the number of cancer deaths has been growing considerably year-to-year according to The World Health Organization [1]. Although many chemotherapeutic agents are already in use, there still are several obstacles to overcome, such as the resistance and side effect associated with anti-cancer drugs [2].

In this context, natural substances emerge as interesting alternatives for cancer treatment, since they usually exhibit good biological and pharmacological properties. Lapachol (2-hydroxy-3-(3-methyl-2-butenyl)-1, 4-naphthoquinone) is a naphthoquinone compound extracted from ipê roxo (*Tabebuia avellanedae*) that is known for its antimicrobial, leishmanicidal, trypanosomicide and antitumor properties [2, 3, 4]. The biological properties of lapachol can be further improved by chemical modification approaches [5].

The synthesis of coordination complexes has been one of the most promising alternatives to enhance the biological properties of lapachol [3, 6–10]. In this sense, coordination compounds containing iron as a central atom are important candidates for metallodrug synthesis due to the biological importance of iron for vital functions [11]. Iron coordination complexes have been investigated also from the bioinorganic point of view, for example, with respect to their antitumor activity [12, 13].

In this work, we report the synthesis of a lapacholate–Fe(II) complex with subsequent characterizations by spectroscopic and electrochemical techniques, as well as computational studies. The

Electronic supplementary material The online version of this article (https://doi.org/10.1007/s11243-020-00427-3) contains supplementary material, which is available to authorized users.

✉ Tamires D. de Oliveira
tamires_tdo@hotmail.com

✉ Ademir dos Anjos
piu_floripa@uems.br

[1] Centro de Desenvolvimento de Tecnologias Químicas - CDTEQ, Universidade Estadual de Mato Grosso do Sul - UEMS, Naviraí, MS, Brazil

[2] PGRN, Universidade Estadual do Mato Grosso do Sul - UEMS, Dourados, MS, Brazil

[3] Faculdade de Ciências Exatas e da Terra, Universidade Federal da Grande Dourados - UFGD, Dourados, MS, Brazil

[4] Faculdade de Ciências Farmacêuticas, Universidade Estadual de Campinas - UNICAMP, Campinas, SP, Brazil

[5] Instituto de Física, Universidade Federal de Mato Grosso do Sul - UFMS, Campo Grande, MS, Brazil

[6] Instituto Federal Goiano - IFG, Ceres, GO, Brazil

antiproliferative activity of the lapacholate–Fe(II) complex against human tumor and non-tumor cell lines was also evaluated.

Experimental

Reagents

The following reagents were of analytical grade and were used as received: iron perchlorate ($Fe(ClO_4)_2 \cdot xH_2O$, ≥ 98 wt.%, Sigma-Aldrich), triethylamine ($N(C_2H_5)_3$, > 99wt.%, Vetec), tetrabutylammonium hexafluorophosphate $N(CH_3CH_2CH_2CH_2)_4(PF_6)$, > 98 wt.%, Sigma-Aldrich), ferrocene ($Fe(C_5H_5)_2$, ≥ 98 wt.%, Sigma-Aldrich), dichloromethane (CH_2Cl_2, ≥ 99%, Vetec), ethanol (CH_3CH_2OH, ≥ 99.8%, Dinâmica), dimethylsulfoxide ($SO(CH_3)_2$, ≥ 99%, Vetec), Trizma® base (2-Amino-2-(hydroxymethyl)-1,3-propanediol, ≥ 99%, Sigma-Aldrich), RPMI-1640 culture medium (Gibco®), penicillin–streptomycin (Sigma-Aldrich), doxorubicin ($C_{27}H_{29}NO_{11}$ HCl, Sigma-Aldrich), fetal bovine serum (Sigma).

Instrumentation and experimental procedures

The melting temperature of the compounds (lapachol and iron(II) complex) was determined using a QUIMIS Q340M13 apparatus. The synthesis of the complex was performed using a QUIMIS Q335D2 ultrasonic bath. CHN elemental analyses were carried out on a Perkin-Elmer CHN2400 equipment. Molar conductivity measurements were performed at 25 °C in CH_2Cl_2 solution (1 mmol L^{-1}) using a Metrohm 912 apparatus. Infrared spectra were collected on a Thermo Nicolet Nexus 650 spectrophotometer with photoacoustic detection accessory using resolution of 8 cm^{-1}. Absorption spectra in the UV–Vis region were obtained in CH_2Cl_2 solution (50 µmol L^{-1}) on a Cary 50 UV–Vis spectrometer. Photoluminescence studies were performed on a Cary Eclipse spectrophotometer with excitation at 295 nm using CH_2Cl_2 solution (64 µmol L^{-1}) as a solvent. Both optical analyses (UV–Vis absorption and photoluminescence) were done using quartz cuvettes (1 cm path length). The electrochemical behavior of the samples was examined by square wave voltammetry using a Metrohm Autolab-PGSTAT 302 potentiostat equipped with an electrochemical cell having one glass-carbon electrode (diameter 2 mm) as the working electrode, Ag/Ag^+ as the reference electrode and a platinum wire in dimethylsulfoxide solution (1 mmol L^{-1}) as the auxiliary electrode. The supporting electrolyte and the internal standard were the tetrabutylammonium hexafluorophosphate salt and the Fc^+/Fc redox pair, respectively [14]. The electronic paramagnetic resonance (EPR) experiments were performed on a Bruker EMX EPR spectrometer with ruby as standard reference at 298 K using DMSO as solvent. The ^1H and $^{13}C\{^1H\}$ NMR analysis of extracted lapachol was carried out on a 14.1 T Bruker Avance 600 MHz spectrometer in $CDCl_3$.

Computational study

All calculations reported in this paper were obtained with the ORCA 2.8 electronic structure program using DFT (B3LYP) levels of theory. The standard 6-31G* basis set was used for all atoms to predict the molecular structure and vibrational wavenumbers, whereas atoms in the ground state were used for complete optimizations, without symmetry constraints [15–17]. Harmonic vibrational wavenumbers were calculated using the analytic second derivatives to confirm the convergence to minima of the potential surface with real vibrational spectra in the gas phase. The absence of imaginary wavenumbers of the calculated vibrational spectra confirms that the structure deduced corresponds to minimum energy [18–21].

TD-DFT calculations were performed by characterizing the energy transitions in low excitation states [17]. The time-dependent density functional theory (TD-DFT) based on the B3LYP/6-31G* method was used to calculate the electronic transitions between occupied and unoccupied states that result in absorption in the UV–Vis range. All structures, IR and UV–Vis spectra, and molecular orbitals were visualized and generated using the Gabedit software [22].

Lapachol extraction

Lapachol was extracted from ipê sawdust [23]. In a typical procedure, 500 mL of CH_2Cl_2 solution was added to 100 g of ipê sawdust and kept under stirring and heating (39 °C) for 30 min. Afterward, the mixture was filtered, and the solution was reduced with a rotary evaporator. The extract was purified by recrystallization from ethanol and water. Yield: 40% relative to the crude extract; melting point: 139 °C; IR data (photoacoustic detection, cm^{-1}): 3351 (*s*), 1643 (*s*), 1662 (*s*), 1050 (*w*), 1271 (*m*), 1593 (*m*), 2973 (*w*), 2854 (*w*), 2912 (*w*). The ^1H and $^{13}C\{1H\}$ NMR of the ligand are present in the supplementary material (Fig. S1).

Synthesis of complex

The synthesis of the $[Fe(Lap)_2(H_2O)_2]$ complex was performed by dissolving 0.55 mmol of lapachol in methanol and adding triethylamine (in the ratio of 1: 1 lapachol: triethylamine) to help in the deprotonation. Afterward, iron perchlorate salt (0.275 mmol) previously solubilized in distilled water was added to the reaction mixture which was kept in an ultrasonic bath for 30 min (Scheme 1). The ensuing red solid was filtered,

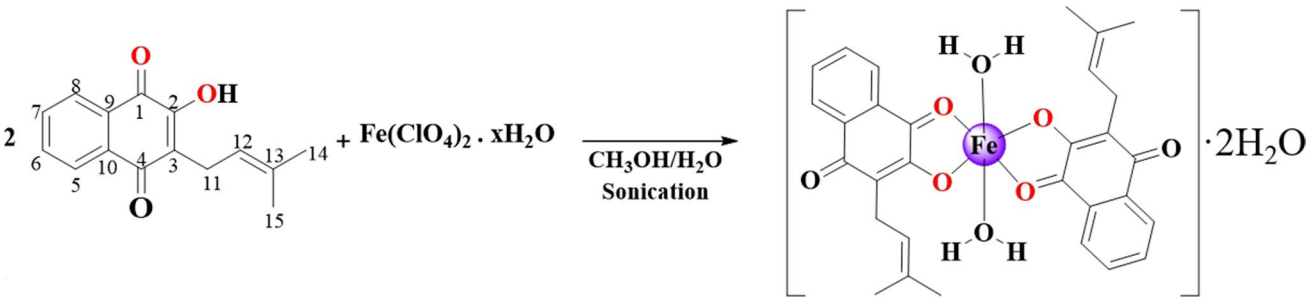

Scheme 1 Pathway for the synthesis of $[Fe(Lap)_2(H_2O)_2]$ complex

washed with a methanol/distilled water solution (1:1 v/v) and dried at room temperature. Yield: 51%; melting point: > 310 °C; elemental analysis for $C_{30}H_{34}O_{10}Fe$ (%) exp. (cal): *C*, 58.73 (59.03); *H*, 5.24 (5.61); *N*, 0.03 (0.00) IR data (photoacoustic detection, cm^{-1}): 1627 (*s*), 1581 (*s*), 1064 (*w*), 1280 (*m*), 3070 (*w*), 2915 (*w*), 2861 (*w*), 732 (*w*).

In vitro antiproliferative assay

The antiproliferative activity of lapachol and $[Fe(Lap)_2(H_2O)_2]\cdot 2H_2O$ complex was evaluated against eight human tumor cell lines (U251 (glioma), MCF-7 (breast tumor line), NCI-ADR/RES (ovary), 786-0 (kidney), NCI-H460 (lung), PC-3 (prostate), OVCAR-03 (ovary), HT-29 (colon)) and one non-tumor cell line (HaCat (keratinocyte)). These cell lines were cultured in 25 cm^3 flasks containing 5 ml of RPMI 1640 medium supplemented with 5% of fetal bovine serum (FBS) and 1% of penicillin–streptomycin (1000 U. mL^{-1}: 1000 µg mL^{-1}) mixture. After 24 h incubation in 96-well plates (100 µL $well^{-1}$), the cell in plate T1 was exposed to the samples (0.25, 2.5, 25 and 250 µg mL^{-1}) in DMSO/RPMI and incubated at 37 °C under 5% CO_2 for 48 h, while cells in plate T0 were fixed with 50% trichloroacetic acid solution (TCA, 50 µL $well^{-1}$). The final DMSO concentration (> 0.25%) did not affect cell viability. Before (T0 plate) and 48 h after (T1 plates) the sample addition, the fixed cells were stained with 0.4% sulforhodamine B in 1% acetic acid solution (50 µL $well^{-1}$) for cell proliferation quantification at 540 nm. The concentration–response curve for each cell line was plotted and, from these curves, the effective concentration TGI (concentration that promotes total growth inhibition) was determined by means of nonlinear regression analysis using Origin 8.0 software. The selectivity index (SI) was calculated by equation $SI = TGI_{HaCat}/TGI_{tumor\ cell\ line}$ using Excel software [24].

Results and discussion

General characterization

The melting point temperature of the pure lapachol ligand was 139 °C. This value is in good agreement with previous reports (139–141 °C) [25]. The complex showed a shift in the melting point temperature compared with the free ligand. The temperature measured for the complex was greater than 300 °C, indicating the coordination of lapachol to the Fe^{2+} ion. The molar conductivity of the complex was 0.262 S m^2 mol^{-1}, suggesting that it was obtained as a neutral compound [26]. The absence of signals in the EPR spectra of the complex confirmed the iron(II) ion in the structure (Fig. S2). The ^1H NMR spectrum of the compound was performed (Fig. 1a), indicating a formation of a low-spin diamagnetic iron(II) complex. It can be observed that the spectrum profile of the metallic complex is similar to the uncoordinated lapachol ligand (Fig.S1), with the absence of a signal at 7.32 ppm (free lapachol), which probably occurs due to the deprotonation of the -OH group of naphthoquinone after coordination to the metallic center. The water molecules are probably overlaid on the signals assigned to the -CH3 groups of the natural ligand, present in the lower frequency region of the spectrum. It is important to emphasize that the integral values of the signals are in agreement with the presence of two Lapachol molecules, according to the proposed structure. To confirm the presence of the hydration and coordination water molecules in the structure of the complex, the thermogravimetric analysis of it was performed. The TG curve of the compound (Fig. 1b) presents two processes of loss of mass, where the first one in 150°C is attributed to the loss of two molecules of hydration water (experimental: 6%; theoretical: 7%), and the second one in 387°C experimental: 85%; theoretical: 75%) to the loss of two molecules of ligands water together with the two molecules of the natural ligand, resulting in a residue of iron(III) oxide.

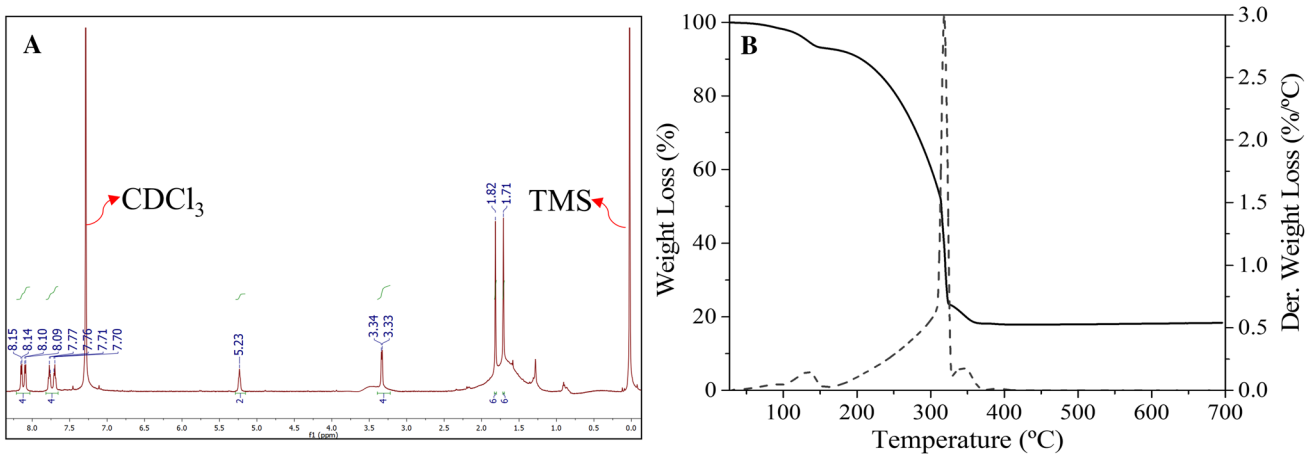

Fig. 1 ^{1}H NMR spectra in $CDCl_3$ (**a**) and TG and DTG profiles from thermogravimetric analysis (**b**)of complex

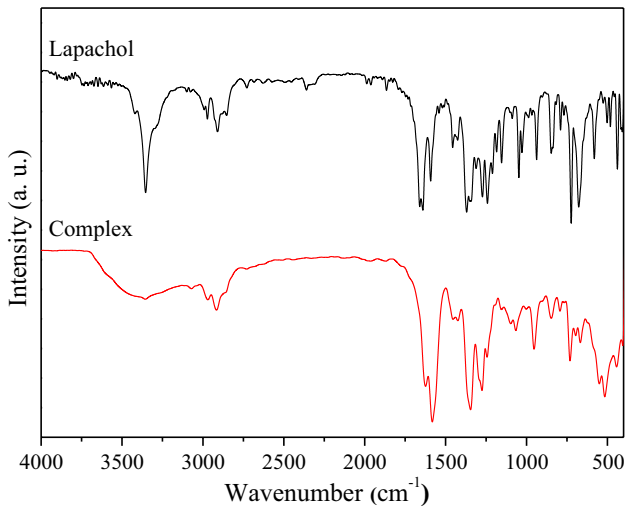

Fig. 2 Infrared spectra of lapachol and ($[Fe(Lap)_2(H_2O)_2]$) complex

Spectroscopic measurements

Infrared

In the infrared spectra (Fig. 2), significant differences can be observed between the vibration bands of the complex and vibration bands of the free ligand. Lapachol has a narrow and strong band at 3351 cm^{-1}, which can be attributed to the stretching of O–H groups. After coordination to the Fe(II) ion, this band is not observed, indicating the coordination of the natural ligand to the metal ion by the phenolic oxygen atom of the naphthoquinone. Another important fact in the structural elucidation of the complex is the presence of a broad band ascribed to water molecules, giving experimental basis for the proposed complex structure. It can also be observed that the band related to the C1=O1 group was shifted in the complex spectrum when compared to the free ligand [1662 cm^{-1} (Lap); 1581 cm^{-1} (complex)]. Accordingly, we can estimate that the coordination to the iron atom is occurring through the carbonyl oxygen (C1=O1), which causes the loss of double bond character, thus causing a significant decrease in the band wavenumber [5, 6, 27, 28]. The band corresponding to the C4=O3 group was also shifted after coordination, but at a less significant extent, as already observed in literature [8, 23, 27]. The other bands present in the complex spectrum also exhibit differences in relation to those in the free ligand spectrum, such as the bands at 2993, 2973, 2912 and 2854 cm^{-1} attributed to stretching of CH (C-12), CH_3 (14 and 15) and CH_2 (C-11) groups, respectively, the band related to CH scissor mode (1369 cm^{-1}) and the out-of-plane vibrations of the aromatic rings (724 cm^{-1}) [5, 23]. These results indicate the bidentate coordination of lapachol to the Fe^{2+} ion through the carbonylic and phenolic oxygens (keto–enol).

UV–Vis spectra

The electronic spectrum of lapachol showed characteristic bands at 223 nm, referring to the transitions π→π* of the aromatic ring, at 249 nm and 282 nm related to the transitions present in the ring that supports the quinonoid system, and at 330 nm attributed to the carbonyl groups characteristic of naphthoquinone (n→π*) [5, 23, 27]. After coordination to the metal ion, there is a shift of the band at 282–278 nm, and the disappearance of the band at 330 nm, which can be directly related to the coordination of the naphthoquinone through the oxygen atom of the C1O1 group. A new low-intensity band at approximately 480 nm (molar absorptivity: 3.612 mol L^{-1} cm^{-1}) was observed in the metal complex spectrum, which could be attributed to ligand-to-metal charge transfer (LMCT) [28, 29]. This new band is also probably related to the red color of the compound. Other changes were related to the intensity of absorption, such

as the hyperchromic effect in the band at 278 nm, for which the metal complex has higher absorbance intensity than the free ligand (molar absorptivity: 31.787 (lap) and 37.659 (complex) mol L^{-1} cm^{-1}). The UV–Vis spectra of the compounds are compared in the supplementary material (Fig. S3).

Emission spectroscopy

Lapachol exhibits an emission band with $\lambda_{max} = 330$ nm from an excitation with wavelength at 255 nm (Fig. 3), which is characteristic of the intra-binding transitions derived from the aromatic ring ($\pi \rightarrow \pi^*$). In the emission spectrum of the complex (Fig. 2), this characteristic band of lapachol is still visible with no displacements in relation to the λ_{max}; however, its luminescence intensity decreased in comparison with the uncoordinated ligand. It is also observed the appearance of a new band in the red region at ~ 566 nm related to the LMCT, demonstrating that the data are in agreement with the absorption spectroscopy results [30]. According to the literature, the coordination of metal ions to fluorophores can lead to two distinct effects, namely the chelation enhanced fluorescence effect (CHEF), in which the luminescence intensity of the ligand increases after coordination, and the chelation enhancement quenching effect (CHEQ), in which the coordination to the metal ion decreases the luminescence intensity of the fluorophore. In this way, it can be suggested that the interaction between lapachol and the iron(II) ion is characterized by the CHEQ effect, demonstrating the effectiveness of the coordination reaction [31].

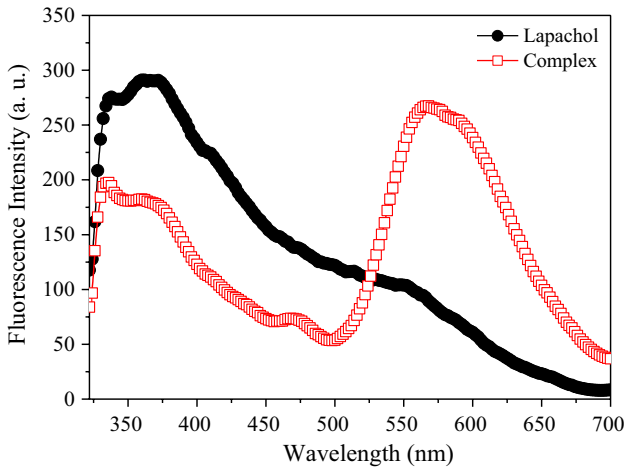

Fig. 3 Fluorescence emission spectra of lapachol and ($[Fe(Lap)_2(H_2O)_2]$) complex

Electrochemical behavior

The electrochemical profile of naphthoquinone compounds is unclear, since they form several species and subspecies. To evaluate the lapachol square wave voltammogram (Fig. 4a), considering a reductive profile, it is initially suggested an electron transfer followed by a protonation step, which may be related to a semiquinone radical formation ($E_{pa4} = 0.767$ V vs. Fc^+/Fc, $E_{pc5} = 0.631$ V vs. Fc^+/Fc). The formation of this reactive radical may lead to the formation of other species, such as anion and dianion radicals ($E_{pc3} = -0.683$ and $E_{pc4} = -0.423$ V vs. Fc^+/Fc). Afterward, catecholate species would be originated ($E_{pa2} = -0.753$ V vs. Fc^+/Fc, $E_{pc2} = -0.947$ V vs. Fc^+/Fc), which can lead to formation of hydroquinone ($E_{pa1} = -1.334$ V vs. Fc^+/Fc; $E_{pc1} = -1.326$ V vs. Fc^+/Fc) through another electronic gain/protonation step. Likewise, there may also occur keto–enol equilibrium, formation of quinone dimeric structure, as well as formation of conjugated bases [32–34].

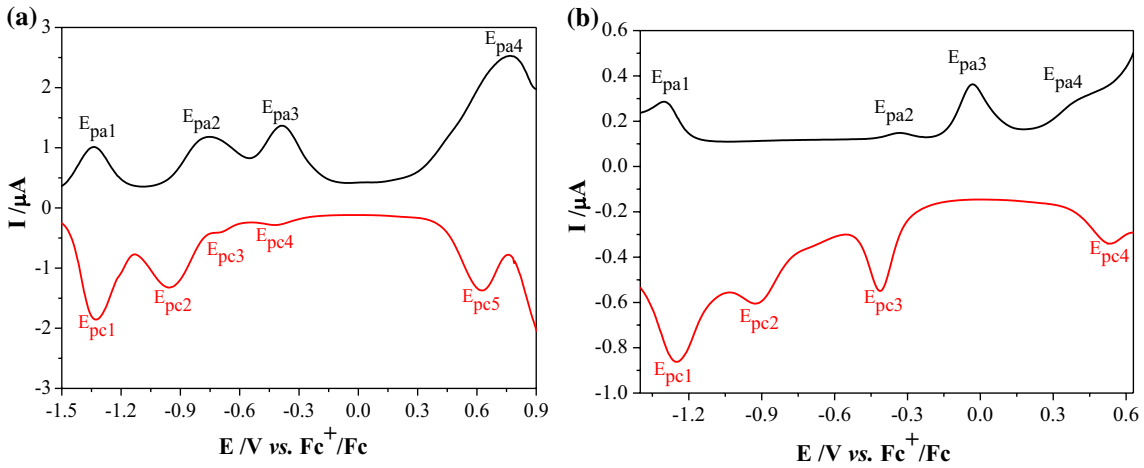

Fig. 4 Square wave voltammograms of lapachol (**a**) and ($[Fe(Lap)_2(H_2O)_2]$) complex (**b**)

In the square wave voltammogram of the complex (Fig. 4b), the first redox pair is attributed to the hydroquinone species ($E_{pa1} = -1.301$ V vs. Fc^+/Fc; $E_{pc1} = -1.252$ V vs. Fc^+/Fc), like observed on the free naphthoquinone. Other processes are related to the ligand and show distinctions due to oxygen→Fe(II) interaction. In the formation of the catecholate species, a low reduction potential and absence of reversibility are observed. This interaction also interferes on the quasi-reversible pair associated with the formation of the semiquinone radical which is shifted to a lower potential ($E_{pa4} = 0.421$ V vs. Fc^+/Fc, $E_{pc4} = 0.532$ V vs. Fc^+/Fc).

Computational details

Full optimization of the $[Fe(lap)_2(H_2O)_2]\cdot 2H_2O$ complex structure was performed with the DFT/B3LYP method in the gas phase and 6-31G* basis set for all atoms. The optimized molecular structure is presented in Fig. 5. Table 1 summarizes the corresponding selected angles and bonding lengths.

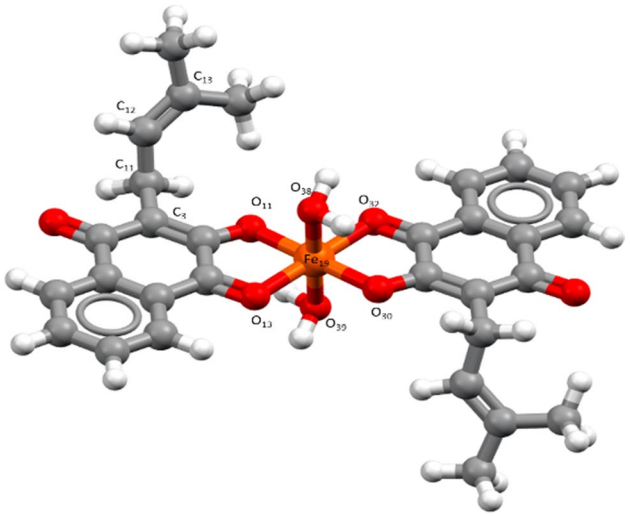

Fig. 5 Optimized structure of the $[Fe(lap)_2(H_2O)_2]$ complex

The Fe(II) metal center is coordinated to the donor atoms O_{11}, O_{13}, O_{30} and O_{32} of the lapachol ligand, as well as to the atoms O_{38} and O_{39} of the water molecules. The complex has a slightly distorted octahedral geometry, as shown by the angles described in Table 1. The bond lengths were calculated as $Fe_{19}–O_{13} = 1.943$ Å, $Fe_{19}–O_{11} = 1.926$ Å for ligand 1 and $Fe_{19}–O_{30} = 1.927$ Å, $Fe_{19}–O_{32} = 1.942$ Å for ligand 2. The bond lengths for the two H_2O molecules are Fe19–O38 = 2.007 Å and Fe19–O39 = 2.006 Å. The angles and bonding lengths are typical of crystalline iron complexes, according to the data available in the CCDC software [35–37].

To estimate the energy associated with the possible conformations of the lapachol lateral groups (*cis* and *trans*), a rotation around a dihedral angle τ (C3–C11–C12–C13) was performed in the interval from 0 to 360° by 20° B3LYP/6-31G * calculations [38]. The PES scan for the lateral group positions presented in Fig. 6 clearly demonstrates the presence of two structures of low energy (I and III) and one of high energy (II). The conformer I is 0.8 kJ mol^{-1} more stable than the conformer III, and the conformer II is at the maximum point in the potential energy curve, having an energy of 20 kJ mol^{-1} greater than the conformer I.

The vibrational modes of the $[Fe(lap)_2(H_2O)_2]\cdot 2H_2O$ complex were also evaluated by the theoretical infrared spectroscopy data (Fig. 7). The frequencies were calculated using the B3LYP/6-31G* method and then scaled by 0.99697 from the correlation between the experimental and computational wavenumbers (Fig. S3). Theoretical infrared data show that the proposed complex structure, with two

Table 1 Selected calculated bond lengths (Å) and bond angles (°) of the $[Fe(lap)_2(H_2O)_2]$ complex structure

Bond	Length (Å)
$Fe_{19}–O_{11}$	1.93
$Fe_{19}–O_{13}$	1.94
$Fe_{19}–O_{30}$	1.93
$Fe_{19}–O_{32}$	1.94
$Fe_{19}–O_{38}$	2.01
$Fe_{19}–O_{39}$	2.01
Angle	**(°)**
$O_{11}–Fe_{19}–O_{13}$	83.3
$O_{11}–Fe_{19}–O_{32}$	96.6
$O_{13}–Fe_{19}–O_{30}$	96.8
$O_{30}–Fe_{19}–O_{32}$	83.3
$O_{38}–Fe_{19}–O_{39}$	179.8

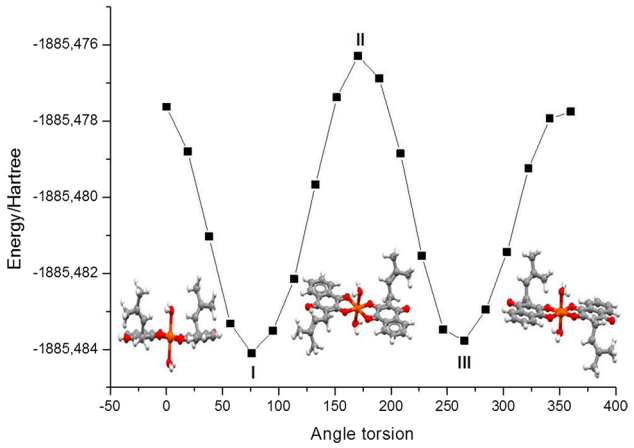

Fig. 6 Potential energy curve of the optimized $[Fe(lap)_2(H_2O)_2]$ complex structure varying the C3–C11–C12–C13 torsion angle, ϕ, from 0° to 360° at intervals of 5° by B3LYP/6-31G* calculations

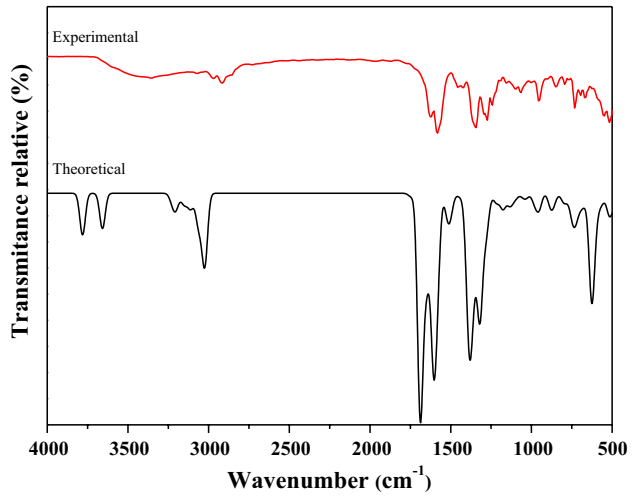

Fig. 7 Theoretical and experimental infrared spectra of $[Fe(lap)_2(H_2O)_2]$ complex. Theoretical data were obtained by the B3LYP/6-31G* method

ligands in the axial position and two aqua ligands in the equatorial position, is consistent with the experimental data.

The energy difference between the HOMO (highest-energy occupied molecular orbital) and LUMO (lowest-energy vacant molecular orbital) orbitals was evaluated because of its importance for the reactivity and stability of the compound. The border orbitals for the $[Fe(Lap)_2(H_2O)_2]\cdot 2H_2O$ complex are shown in Fig. 8 (Table S1) [39, 40].

The energy values calculated for the HOMO and LUMO at the DFT level were 0.176690 au and − 0.112020 au, respectively; therefore, the band gap energy value is 0.06467 au (169,8 kJ mol^{-1}). The vacuum UV–Vis spectrum displayed three main absorption bands with maximum wavelength at 251, 280 and 489 nm, corroborating with

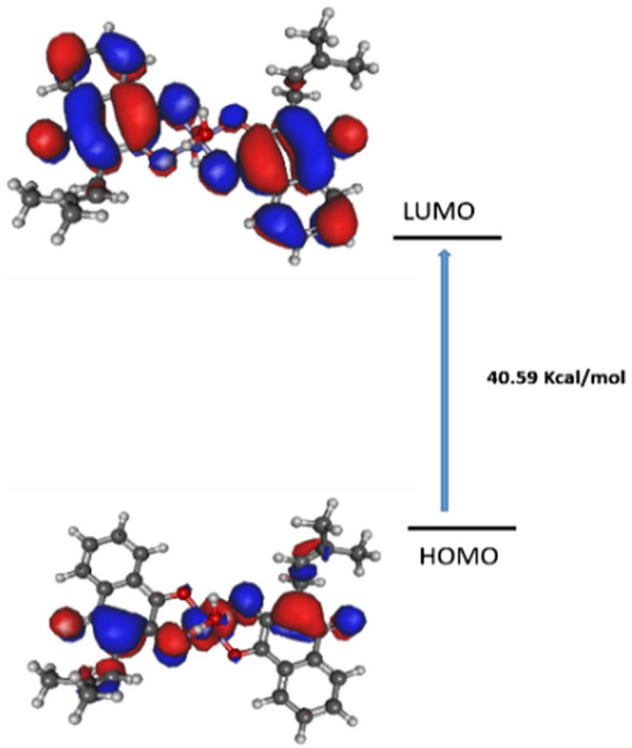

Fig. 8 Energy level diagram. The HOMO/LUMO plots of $[Fe(lap)_2(H_2O)_2]$ complex with indication of the HOMO–LUMO gap

the experimental spectrum (Fig. S3). The theoretical data are also in agreement with the experimental assignments: the absorption band at 251 nm (251 nm exp.) attributed to a π–π type transition formed by the contribution of the HOMO-7 → LUMO + 4 transition by 25.17% and HOMO-4 → LUMO + 4 transition by 32.84%, and with significant contribution of the naphthoquinone carbonyl group orbitals. The n–π type absorption band at 280 nm (278 nm exp.) formed mainly by the HOMO → LUMO + 5 and HOMO → LUMO + 7 transitions with contributions of 10.87% and 14.01%, respectively. The LMCT-type absorption band at 489 nm (480 nm exp.) is attributed to HOMO-7 → LUMO transition (contribution of 35.99%) and HOMO-6 → LUMO transition (contribution of 32.62%).

In vitro antiproliferative assay

The in vitro antiproliferative assay of lapachol and $[Fe(Lap)_2(H_2O)_2]\cdot 2H_2O$ complex was performed following the Developmental Therapeutics Program NCI/NIH protocol (Fig. 9) [41]. Considering the concentration required to total cell growth inhibition (TGI), it was possible to observe that the coordination to the Fe(II) ion remarkably increased the antiproliferative effect of lapachol, since the complex was very effective against all tumor cell lines. The complex presented the best results for the U251

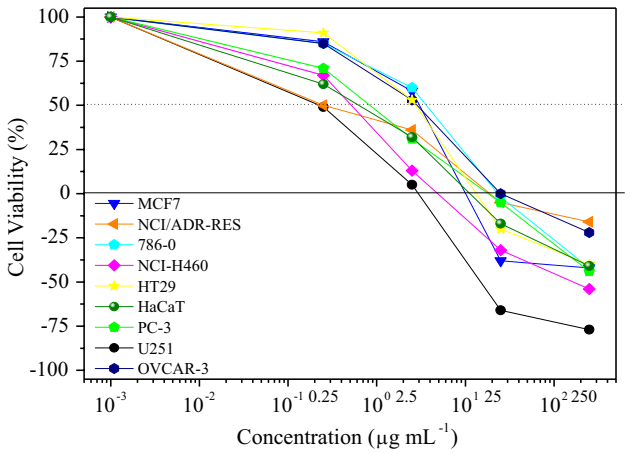

Fig. 9 Correlation between the percentage of cell growth and the concentration of the complex $[Fe(Lap)_2 (H_2O)_2]$

(glioma, TGI = 3.60 µmol L^{-1}) and NCI-H460 (lung, TGI = 10.65 µmol L^{-1}) lines, with a selectivity index (SI) of 6.46 and 2.18, respectively, in comparison with the TGI value observed for the non-tumoral cell line HaCat (Table 2). It is important to highlight that the selectivity index (SI) is an indicator of potential antiproliferative effects on normal tissues; however, as an on-target toxicology approach (the expected drug effect), SI does not predict other systemic effects [24].

Other lapachol-based complexes described in the literature also showed higher antitumor activity than the free naphthoquinone, but the structures of these compounds are quite different from the $[Fe(lap)_2(H_2O)_2]\cdot 2H_2O$ complex presented in the work, mainly because lapachol was not the only ligand used in the metal complex synthesis [3, 8]. In this case, the TGI values given in Table 2 are relevant from a bioinorganic chemistry point of view, since the complex evaluated was only comprised of lapachol. These results demonstrate that coordination chemistry may be a powerful approach for new anti-cancer drug development.

Conclusions

A new coordination complex containing lapachol and Fe(II) ion was synthesized and characterized by spectroscopic techniques. The theoretical study on the compound structure was carried out for complementing and confirming the experimental results, demonstrating the coordination of lapachol to the Fe(II) central atom in a keto–enolic way. The results of antiproliferative activity against several tumor cell lines demonstrated that the coordination to the metal ion substantially enhanced the antitumor activity of lapachol. The complex was very active for all the tumor cell lines, being particularly effective against the tumoral lineage of glioma (U251), presenting lower TGI value in comparison with the non-tumoral lineage. The results obtained are relevant from the bioinorganic point of view since they demonstrate the potential of coordination chemistry in the development for new, effective compounds for cancer treatment.

Table 2 Antiproliferative activity, expressed as TGI values (µmol L^{-1}) and selective index (SI) for lapachol, $[Fe(Lap)_2(H_2O)_2]$ complex and doxorubicin standard

Cell line	Lapachol		Complex		Doxorubicin	
	TGI	SI	TGI	SI	TGI	SI
U251	39.21	2.20	N3.60	6.46	0.29	1.00
MCF-7	133.7	0.65	25.06	0.93	2.02	0.14
NCI-ADR/RES	236.5	0.36	62.41	0.37	2.21	0.13
786-0	322.37	0.27	51.44	0.45	1.20	0.24
NCI-H460	52.83	1.63	10.65	2.18	0.57	0.51
PC-3	123.8	0.70	30.14	0.77	0.75	0.39
OVCAR-03	91.63	0.94	78.79	0.30	2.58	0.11
HT29	163.0	0.53	35.55	0.65	5.15	0.06
HaCat*	86.27	–	23.26	–	0.29	–

TGI concentration required for totally cell growth inhibition; *SI* selectivity index expressed as $TGI_{HaCat}/TGI_{tumor\ cell\ line}$

Human tumor cell lines: U251 = Glioma; MCF-7 = Breast; NCI-ADR/RES = Ovary, expressing multidrug resistance phenotype; 786-0 = Kidney; NCI-H460 = Lung, non-small cells; PC-3 = Prostate; OVCAR-03 = Ovary; HT-29 = Colon. Human non-tumor cell line: HaCa t = Keratinocyte

Acknowledgements The authors are grateful to the Coordination of Improvement of Higher Education Personnel (CAPES)—Finance Code 001, the Foundation for the Development of Education, Science and Technology of the State of Mato Grosso do Sul (FUNDECT), and the National Council for Scientific and Technology Development (CNPq) for their financial support.

References

1. World Health Organization. Cancer. https://www.who.int/health-topics/cancer#tab=tab_1. Accessed 9 Sep 2020
2. Brücher BLDM, Lyman G, Van HR et al (2014) Imagine a world without cancer. BMC Cancer 14:1–8
3. de Oliveira LG, Silva MM, de Paula FCS et al (2011) Antimony(V) and bismuth(V) complexes of lapachol: synthesis, crystal structure and cytotoxic activity. Molecules 16:10314–10323. https://doi.org/10.3390/molecules161210314
4. Ferraz PAL, de Abreu FC, Pinto AV et al (2001) Electrochemical aspects of the reduction of biologically active 2-hydroxy-3-alkyl-1,4-naphthoquinones. J Electroanal Chem 507:275–286
5. Caruso F, Martínez AM, Rossi M, Goldberg A, Villalba MEC, Aymonino PJ (2009) Crystal and molecular structure of manganese(II) lapacholate, a novel polymeric species undergoing temperature-reversible metal to ligand electron transfer. Inorg Chem 48:3529–3534. https://doi.org/10.1021/ic8015194
6. Parrilha GL, Vieira RP, Campos PP et al (2012) Coordination of lapachol to bismuth(III) improves its anti-inflammatory and anti-angiogenic activities. Biometals 25:55–62. https://doi.org/10.1007/s10534-011-9481-y
7. Kandioller W, Balsano E, Meier SM et al (2013) Organometallic anticancer complexes of lapachol: metal centre-dependent formation of reactive oxygen species and correlation with cytotoxicity. Chem Commun (Camb) 49:3348–3350. https://doi.org/10.1039/c3cc40432c
8. Oliveira KM, Corrêa RS, Barbosa MIF et al (2017) Ruthenium(II)/triphenylphosphine complexes: an effective way to improve the cytotoxicity of lapachol. Polyhedron 130:108–114. https://doi.org/10.1016/j.poly.2017.04.005
9. Barbosa MIF, Corrêa RS, Mara K et al (2014) Antiparasitic activities of novel ruthenium/lapachol complexes. J Inorg Biochem 136:33–39. https://doi.org/10.1016/j.jinorgbio.2014.03.009
10. Oliveira KM, Peterson EJ, Carroccia MC et al (2020) Ru(II)-naphthoquinone complexes with high selectivity for triple-negative breast cancer. Dalton Trans 2020:1–12. https://doi.org/10.1039/d0dt01091j
11. Gupta CP (2014) Role of iron (Fe) in body. J Appl Chem 7:38–46
12. Wani WA, Baig U, Shreaz S et al (2016) Recent advances in iron complexes as potential anticancer agents. New J Chem 40:1063–1090. https://doi.org/10.1039/c5nj01449b
13. Estrada-Montaño AS, Ryabov AD, Gries A et al (2017) Iron(III) pincer complexes as a strategy for anticancer studies. Eur J Inorg Chem 2017:1673–1678. https://doi.org/10.1002/ejic.201601350
14. Gagne RR, Koval CA, Lisensky GC (1980) Ferrocene as an internal standard for electrochemical measurements. Inorg Chem 19:2854–2855. https://doi.org/10.1021/ic50211a080
15. Neese F (2012) The ORCA program system. WIREs Comput Mol Sci 2:73–78. https://doi.org/10.1002/wcms.81
16. Amini M, Arab A, Derakhshandeh PG et al (2014) A novel iron complex containing an N, O-type bidentate oxazoline ligand: synthesis, X-ray studies, DFT calculations and catalytic activity. Spectrochim Acta Part A Mol Biomol Spectrosc 133:432–438. https://doi.org/10.1016/j.saa.2014.06.012
17. Devi PP, Chipem FAS, Singh CB, Lonibala RK (2019) Complexation of 2-amino-3-(4-hydroxyphenyl)-N′-[(2-hydroxyphenyl) methylene] propane hydrazide with Mn(II), Co(II), Ni(II), Cu(II) and Zn(II) ions: structural characterization, DFT, DNA binding and antimicrobial studies. J Mol Struct 1176:7–18. https://doi.org/10.1016/j.molstruc.2018.08.070
18. Sama F, Raizada M, Ashafaq M et al (2019) Synthesis, structure and DNA binding properties of a homodinuclear Cu(II) complex: an experimental and theoretical approach. J Mol Struct 1176:283–289. https://doi.org/10.1016/j.molstruc.2018.08.081
19. Szabó L, Herman K, Mircescu NE et al (2014) Surface-enhanced Raman scattering and DFT investigation of 1,5-diphenylcarbazide and its metal complexes with Ca(II), Mn(II), Fe(III) and Cu(II). J Mol Struct 1073:10–17. https://doi.org/10.1016/j.molstruc.2014.02.044
20. Üstün E, Koç Ş, Demir S, Özdemir I (2016) Carbon monoxide-releasing properties and DFT/TDDFT analysis of $[Mn(CO)_3(bpy)L]PF_6$ type novel manganese complexes. J Organomet Chem 815–816:16–22. https://doi.org/10.1016/j.jorganchem.2016.05.001
21. Üstün E, Demïr S, Coşkun F et al (2016) A theoretical insight for solvent effect on myoglobin assay of $W(CO)_4L_2$type novel complexes with DFT/TDDFT. J Mol Struct 1123:433–440. https://doi.org/10.1016/j.molstruc.2016.07.002
22. Allouche A-R (2011) Gabedit-A graphical user interface for computational chemistry softwares. J Comput Chem 32:174–182. https://doi.org/10.1002/jcc
23. Farfán RA, Espíndola JA, Gomez MI et al (2012) Structural and spectroscopic properties of two new isostructural complexes of lapacholate with cobalt and copper. Int J Inorg Chem 2012:1–6. https://doi.org/10.1155/2012/973238
24. Muller PY, Milton MN (2012) The determination and interpretation of the therapeutic index in drug development. Nat Rev 11:751–761
25. Epifano F, Genovese S, Fiorito S et al (2013) Lapachol and its congeners as anticancer agents: a review. Phytochem Rev 13:37–49
26. Geary WJ (1971) The use of conductivity measurements in organic solvents for the characterisation of coordination compounds. Coord Chem Rev 7:81–122. https://doi.org/10.1016/S0010-8545(00)80009-0
27. Martínez MA, de Jiménez MCL, Castellano EE et al (2003) Synthesis, structure and properties of a zinc(II) complex with the lapacholate anion and ethanol as ligands. J Coord Chem 56:803–816. https://doi.org/10.1080/0095897031000113959
28. Farfán RA, Espíndola JA, Martínez MA et al (2009) Synthesis and crystal structure of a new lapacholate complex with nickel(II), $[Ni(Lap)_2(DMF)(H_2O)]$. J Coord Chem 62:3738–3744. https://doi.org/10.1080/00958970903207351
29. Farfán RA, Espíndola JA, Gomez MI, de Jiménez MCL, Piro OE, Castellano EE, Martínez MA (2015) Crystal structure, spectroscopic and thermal properties of $[Zn(Lap)_2(DMF)(H_2O)]$ and isomorphous $[M(Lap)_2]_n$ (M: Cd, Mn) complexes. J Mol Struct 2:80–87. https://doi.org/10.1016/j.molstruc.2015.01.042
30. Huang T, Zhang M (2014) Novel copper(I) complexes with extended π…π interactions: synthesis, structure, characterization and spectroscopic properties. Inorg Chim Acta 416:28–34. https://doi.org/10.1016/j.ica.2014.03.011
31. Formica M, Fusi V, Giorgi L, Micheloni M (2012) New fluorescent chemosensors for metal ions in solution. Coord Chem Rev 256:170–192. https://doi.org/10.1016/j.ccr.2011.09.010
32. Goulart MOF, Lima NMF, Sant'Ana AEG, Ferraz PAL, Cavalcanti JCM, Falkowski P, Ossowski T, Liwo A (2004) Electrochemical studies of isolapachol with emphasis on oxygen interaction with its radical anions. J Electroanal Chem 566:25–29. https://doi.org/10.1016/j.jelechem.2003.10.043

33. De Lucas NC, Ferreira ABB, Netto-ferreira JC (2015) Fotoquímica de naftoquinonas. Rev Virtual Quím 7:403–463
34. Kathawate L, Shinde Y, Yadav R, Kasabe U, Nikalje M, Salunkegawali S (2014) Thermal and spectral properties of alkali metal complexes of 2-hydroxy-1, 4-naphthoquinone. J Therm Anal Calorim 115:2319–2330. https://doi.org/10.1007/s10973-013-3204-2
35. England J, Gondhia R, Bigorra-lopez L et al (2009) Towards robust alkane oxidation catalysts: electronic variations in non-heme iron(II) complexes and their effect in catalytic alkane oxidation. Dalton Trans 2009:5319–5334. https://doi.org/10.1039/b901390c
36. Garge P, Chikate R, Padhye S et al (1990) Iron(II) complexes of ortho-functionalized p-naphthoquinones. 2. Crystal and molecular structure of bis(aquo)bis(lawsonato)iron(II) and intermolecular magnetic exchange interactions in bis(3-aminolawsonato)iron(II). Inorg Chem 29:3315–3320. https://doi.org/10.1021/ic00343a012
37. Bittner MM, Kraus D, Lindeman DSV et al (2013) Synthetic, spectroscopic and DFT studies of iron complexes with iminobenzo(semi)quinone ligands: implications for o-aminophenol dioxygenases. Chemistry (Easton) 19:9686–9698. https://doi.org/10.1002/chem.201300520.Synthetic
38. Kozlowski D, Trouillas P, Calliste C et al (2007) Density functional theory study of the conformational, electronic, and antioxidant properties of natural chalcones. J Phys Chem 111:1138–1145
39. Saureu S, De GC (2016) TD-DFT study of the light-induced spin crossover of Fe(III) complexes. Phys Chem Chem Phys 18:1233–1244. https://doi.org/10.1039/c5cp06620d
40. Kirgan RA, Rillema DP (2007) Computational study of iron(II) systems containing ligands with nitrogen heterocyclic groups. J Phys Chem 111:13157–13162. https://doi.org/10.1021/jp076334t
41. Monks A, Scudiero D, Skehan P et al (1991) Feasibility of a high-flux anticancer drug screen using a diverse panel of cultured human tumor cell lines. J Natl Cancer Inst 83:757–766. https://doi.org/10.1093/jnci/83.11.757